Multimodal barometric and inertial measurement unit based tactile sensor for robot control

Gorkem Anil AL and Uriel Martinez-Hernandez

***Abstract*— In this paper, we present a low-cost multimodal tactile sensor capable of providing accelerometer, gyroscope and pressure data using a 7-axis chip as sensing element. This approach reduces the complexity of tactile sensor design and collection of multimodal data. The tactile device is composed of a top layer (a printed circuit board and sensing element), a middle layer (soft rubber material), and bottom layer (plastic base) forming a sandwich structure. This approach allows the measurement of multimodal data when force is applied on different parts of the top layer of the sensor. The multimodal tactile sensor is validated with analyses and experiments in both offline and real-time. First, the spatial impulse response and sensitivity of the sensor are analysed with accelerometer, gyroscope and pressure data systematically collected from the sensor. Second, estimation of contact location from a range of sensor positions and force values is evaluated using accelerometer and gyroscope data together with a Convolutional Neural Network (CNN) method. Third, the estimation of contact location is used to control the position of a robot arm. The results show that the proposed multimodal tactile sensor has the potential for robotic applications such as tactile perception for robot control, human-robot interaction and object exploration.**

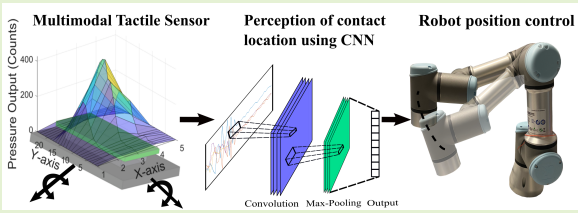

***Index Terms*— Multimodal tactile sensor, CNN based contact recognition, robot control**

I. Introduction

ROBOTS offer a tremendous potential for interaction and collaboration with humans and other robots to perform tasks efficiently and safely such as assembly, telemanipulation, assistance and healthcare [1], [2]. These robots need to be capable of physically sensing and perceiving their surrounding environment to make reliable decisions, actions and avoid collisions that can harm humans and other robots [3]. Tactile sensing is an essential component that needs to be considered in the design and development of robots to allow them to physically explore their surrounding environment for safe interaction with humans and other robots, detection of contact, recognition and manipulation of objects [4], [5].

Tactile sensors have been studied taking inspiration from the human sense of touch, which can respond to stimuli such as pressure, vibration, deformation and temperature [6]. Particularly, researchers have focused on biomimetic fingertips and skin for robotic grippers, dexterous robot hands and for the torso and arms of humanoids to perform object manipulation and recognition, human-robot interaction tasks [7]. These tactile sensors tend to combine different sensing elements to obtain multiple data formats, e.g., pressure and vibration, that mimic the stimuli from the sense of touch [8]. However, the use of multiple sensing elements in a tactile sensor, makes its design and fabrication complex and costly.

To tackle these challenges, we present a low cost multimodal tactile sensor for contact detection, recognition of contact location and robot control. This work contributes to the field of tactile sensing with a novel multimodal tactile sensor that requires only one chip (sensing element) to provide pressure, accelerometer and gyroscope data. The use of one chip reduces the complexity of sensor design and multimodal data acquisition. The tactile sensor is built using a sandwich structure which increases the spatial impulse response.

The performance of the multimodal tactile sensor is validated with various experiments in offline and real-time modes. First, the sensitivity across the tactile device is analysed using pressure data systematically collected by applying repetitive force with a robotic platform on the sensor. Second, accelerometer and gyroscope data obtained by applying different force values on the tactile sensor are used, together with a Convolutional Neural Network (CNN), for recognition of contact location. This experiment is performed in offline and real-time modes to show that the sensor can detect contact location accurately from a sensing area larger than the size of the chip. Third, a robot arm is controlled to move to specific positions on a grid based on the contact location recognised when a human applies force on the multimodal sensor. The design, analysis and validation processes show that this sensor can provide rich multimodal data for sensing, perception and control in robotic applications.

This paper is organised as follows: Section II presents the

*This work was supported by The Republic of Turkey Ministry of National Education.

Gorkem and Uriel are with the inte-R-action Research Lab, the Centre for Autonomous Robotics (CENTAUR), Department of Electronic and Electrical Engineering, Faculty of Engineering and Design, University of Bath, UK (gga31, u.martinez)@bath.ac.uk

related work. The sensor design and performance analysis are described in Section III. Offline and real-time experiments are presented in Section IV. Sections V and VI present the discussion and conclusions, respectively.

II. Related Work

Tactile sensors designed and developed using different transduction technologies and data processing methods for robotic applications are presented in this section.

Capacitive technology has been used to develop tactile sensors that require large dynamic range, high spatial resolution and sensitivity. This technology has been used in robots such as the iCub humanoid skin [9], the gripper of PR2 robot [10], and soft fingertips of RobotiQ gripper [11]. Capacitive sensing is commonly affected by hysteresis, and requires relatively complex measurement systems [12].

Piezo technology has been used for piezoresistive and piezoelectric tactile sensors for robot fingers and palms to recognise deformable and rigid objects [13], to detect slippage [14] and as array of sensors in robot hands for object recognition based on the object size and stiffness [15]. Tactile sensors with piezo technology are relatively easy to build, low cost, and can provide high sensitivity and high frequency. However, hysteresis, reproducibility and susceptability to slight changes in temperature limit their application [12].

Optical systems offer a solution that rely on fiber optics and cameras for tactile sensors. Arrays of optical fibers and fiber Bragg grating have been used in robotic finger designs [16]. Soft skin with embedded cameras has been employed in robot hands for force estimation and object slippage detection [3]. TacTip fingertip uses a camera covered with a soft skin for robotic applications such as object exploration and manipulation [17]. This technology provides high spatial resolution, repeatability and sensitivity, but they are limited by large sensor size, high power consumption, computational cost and susceptible to light conditions [7].

Magnetic technology has been used to build tactile sensors for measuring three-dimensional force based on the Hall effect [18]. Soft tactile sensors with magnetic technology have also been used for detection of light touch and shear forces [19]. Magnetic tactile sensors offer high sensitivity, linear response and physical robustness, but their performance is affected by the magnetic field of nearby electrical devices [8].

Barometric modules can be embedded in rubber to build soft tactile sensors to provide pressure output with high sensitivity and linearity [20]. Arrays of barometric modules have been used in robotic applications such as footpads for running robots [21], estimation of ground forces and centre of pressure in robotic legs [22], and on robotic hands and fingers to estimate material stiffness [23]. This technology allows to build low-cost and small size tactile sensors, but they are limited by low frequency response.

The use of multiple integrated circuits or chips in the design of tactile sensors to mimic human tactile sensing abilities has shown improvements in robotic applications for object detection, recognition, and manipulation. The BioTac fingertip composed of multiple sensing elements is capable of providing contact information, temperature and vibrations [24]. A bio-inspired multimodal tactile sensor embedded with pressure, magnetic, angular velocity and acceleration sensors has been used for profile and object recognition [25]. Multimodal data from an inertial measurement unit (IMU) and pressure sensor in a tactile device have been used for detection of contact force and surface orientation [26]. HEX-O-SKIN is a multimodal tactile module consisting of proximity, accelerometer and thermistor sensors designed for safe robot interaction [27]. Surface classification has been performed using an array of seven force sensors and five accelerometers embedded in a biomimetic fingertip sensor [28]. Even though tactile devices with multimodal sensing elements provide rich information for a variety of robotic applications, the combination of different sensing elements poses challenges. For example, the integration of multiple sensors increases the complexity of design and wiring, the fabrication cost, and requires complex acquisition boards and programs for multimodal data collection.

Tactile sensors have been used with computational methods for data processing, feature extraction, classification and robot control. Data from soft fingertip sensors with embedded cameras have been processed for feature extraction, recognition and exploration tasks using methods such as Principal Component Analysis (PCA) and Convolutional Neural Networks (CNN) [29], [30]. Recognition of touch on robot skin for human-robot interaction tasks has been studied using Support Vector Machines, Dynamic Bayesian Networks (DBN) and Gaussian Processes (GP) with the Baxter robot and iCub humanoid skin [31], [32]. Self-Organising Maps (SOM), k-Nearest Neighbour (kNN), Artificial Neural Networks (ANN) and DBNs have been used for detection of contact location and object shape extraction using biomimetic tactile robot hands and fingers [33]–[35]. Intelligent tactile sensing for object exploration and robot control has been studied using pressure and piezoresistive sensor arrays with CNN and Deep Convolutional Neural Networks [36], [37].

The paper proposes a multimodal tactile sensor that uses only one chip to provide accelerometer, gyroscope and pressure data. This approach contributes to reducing the complexity of design, sensor size and cost of fabrication. A CNN method is used for tactile data processing to exploit the sensor capability for contact detection, recognition of contact location and robot control. The detailed description of the proposed soft multimodal tactile sensor is presented in the next sections.

III. Methods

A. Sensor Package and Electrical Design

The sensing element of the tactile sensor uses the 7-axis ICM-20789 device (TDK InvenSense) which consists of 3-axis gyroscope, 3-axis accelerometer and a barometric pressure sensor. This device has dimensions of $4\,\text{mm}\times4\,\text{mm}\times1.4\,\text{mm}$ and offers two data transfer options: 400 kHz I2C communication for accelerometer, gyroscope and pressure sensors and 8 MHz SPI for acceleometer and gyroscope sensors. The barometric sensor consumes less power than any other barometric sensor in the market. The pressure sensor operates between 30 kPa and 110 kPa, and data can be collected in four

different modes in terms of current and noise; Low Power (3.2 Pa noise, 1.3μA), Normal (1.6 Pa noise, 2.6μA), Low Noise (0.8 Pa noise 5.2μA), and Ultra Low Noise (0.4 Pa noise 10.4μA). The ICM-20789 device with orientation axes, and the block diagram of gyroscope, accelerometer and pressure sensors are shown in Figures 1A and 1B, respectively.

The ICM-20789 chip is soldered on a QFN/QFP PCB (socket with 0.5 mm pitch and 30×15 mm size) as follows. First, a 24 pin steel stencil is placed on the PCB. Second, Loctite LF 318 96SCAGS88.5V solder paste is spread on the stencil avoiding the excess of paste between or around pads. Third, the chip is placed gently on the PCB and aligned to the orientation of the socket using an electronic microscope (Figure 1C). Finally, the PCB and sensor are placed in a reflow oven with the temprature set at 250° to solder the chip correctly. The I2C communication protocol is used to transfer data from accelerometer, gyroscope and pressure sensors to a microcontroller board. Figure 1D shows the circuit diagram needed to set the correct signals for synchronisation and data transferring from the ICM-20789 sensor to an Arduino Mega2560 board. These data are then transferred to a workstation using the Robot Operating System (ROS) for posterior analysis and robot control as described in next sections.

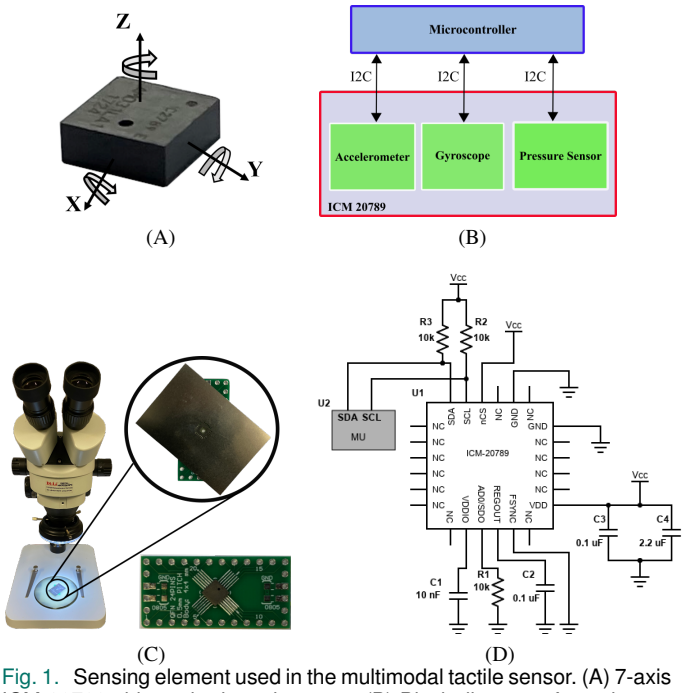

Fig. 1. Sensing element used in the multimodal tactile sensor. (A) 7-axis ICM-20789 chip and orientation axes. (B) Block diagram of accelerometer, gyroscope and pressure sensors. (C) ICM-20789 chip placed on a PCB using a stencil and electronic microscope. (D) Schematic for data transfer with I2C communication protocol.

B. Tactile Sensor Design

The PCB and sensor are covered with a rectangular soft case made of Ecoflex 00-30 silicon material. The design and fabrication process of this soft case is as follows. First, same amount of Ecoflex rubbers are mixed in a small glass. Second, the rubber is degassed using a vacuum chamber to reduce the air bubble that can affect the material behaviour. Third, the rubber is poured in a 3D printed mold to fabricate the rectangular case, and cured for 5 hours at room temperature. Fourth, the soft case is glued on the PCB using a strong adhesive (Figure 2A). Finally, the soft case glued on a plastic base to form a sandwich structure. This process is shown in Figure 2B. The soft case with dimensions of 24 mm×11.5 mm×4.5 mm covers the area of the PCB that can be used efficiently. The chip is covered with silicon material leaving a 0.5 mm gap between the top of the chip and the inner layer of the case, preventing the possibility of contacting with the silicone before applying a force on the sensor. When a force is applied on the tactile sensor, the silicon material compresses, touching the chip and generating pressure data from the barometric sensor.

C. Sensor Performance

The spatial impulse response of the multimodal tactile sensor is analysed using sensor data when force is systematically applied with a tapping exploratory procedure performed employing the Universal Robot (UR3) arm and a 10 mm spherical tip (Figure 3B). For this process, an extension board is mounted on the tactile sensor to connect to the circuitry responsible for data transfer using I2C communication protocol. The tactile sensor is covered with an elastic fabric to avoid slippage during the data collection (Figure 3A). The tapping process is performed on an array of 3 columns×24 rows (72 sensor locations in total) with 1 mm step size on y axis and 3.5 mm step size on x axis, and duration of 3 s per tap (Figures 3A and 3C). The tapping process is repeated 5 times in a range of contact depths from 0.2 mm to 1.6 mm with 0.2 mm steps. Sensor data are collected in Low Noise mode (0.8 Pa noise, 5.2 μA) using an Arudino Mega 2560 and ROS with 30 Hz sampling frequency. The force applied on the sensor is measured using the FT-300 force/torque sensor with 180 Hz sampling frequency.

Examples of mean pressure and measured force collected at different contact depths are shown in Figure 4. The data represented by blue, red and green lines correspond to the first (blue), second (red) and third (green) columns, respectively, along 24 rows on the sensor as shown in Figure 3A. Pressure data from the tactile sensor was able to be measured from a contact depth of 0.8 mm. In this contact depth, the highest pressure output and measured force are observed in the second column of the sensor (red colour line) in Figure 4. These data show that when a force is applied near to or at the centre of the sensor (contact points 12, 13 and 14 in Figures 4A and 4C), a large contact between the chip and the silicon material results in a large pressure output. When the force is applied near to or at the edge of the sensor (e.g., contact points 22, 23, and 24), it bends, reducing the contact between the silicon material and the chip which results in a lower pressure output. Moreover, when the contact depth increases, the sensor can detect more contact points along the 24 rows or positions used for data collection. For example, with 0.8 mm contact depth the sensor provides pressure data between positions 8 and 19 along the sensor (Figure 4A), while at 1.6 mm contact depth, pressure data is available between positions 4 to 24 (Figure 4C). When a contact is applied on the centre locations of the tactile sensor, the silicon shows high resistance resulting in large measured forces. However, if a contact is applied near to or at the edges

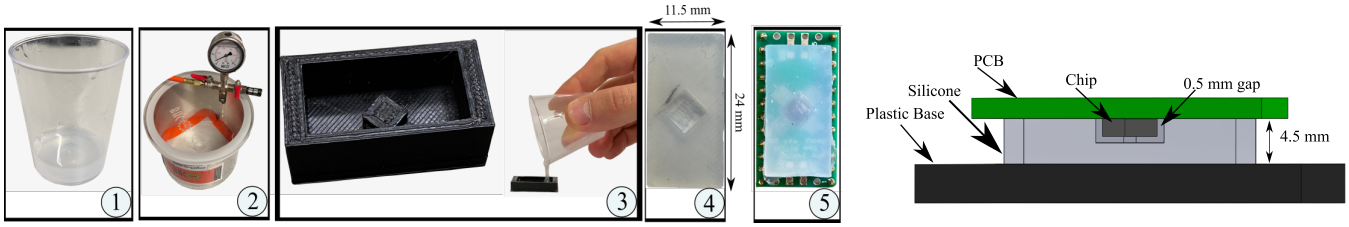

Fig. 2. Fabrication process of the multimodal tactile sensor. (A) Steps for fabrication of the soft rectangular case of the sensor: 1) rubber liquids are mixed, 2) material degassing using a vacuum chamber, 3) rubber is poured in the mould to form a rectangular case, 4) cured soft rectangular case, 5) chip covered with the soft case. (B) Soft case attached on the PCB and mounted on a plastic base creating a sandwich configuration.

of the tactile sensor, this bends and the resistance of the silicon decreases resulting in lower measured forces. This behaviour is observed in the examples of measured forces at the centre and edge contact points in Figures 4B and 4D.

Examples of accelerometer and gyroscope data from the tapping process described previously are shown in Figure 5. These figures illustrate mean accelerometer and gyroscope signals in x and y axes along 24 rows and columns 1 to 3 for contact depths of 0.8 mm and 1.6 mm. Accelerometer signals in x axis change from positive to near zero values in column 1, from positive to negative values in column 2, and from near zero to negative values in Column 3. Opposite output signals are observed for accelerometer in y axis. The amplitude of gyroscope signals in x axis changes from zero to positive and negative values gradually in Column 1, between positive and negative values in Column 2, and from positive and negative values to zero in Column 3. Opposite output trends are observed for gyroscope in y axis in Column 1 and Column 3 for taps along 24 rows, and similar change in Column 2.

The analysis of the spatial response shows that the highest sensitivity is achieved at contact positions 13 and 14, where

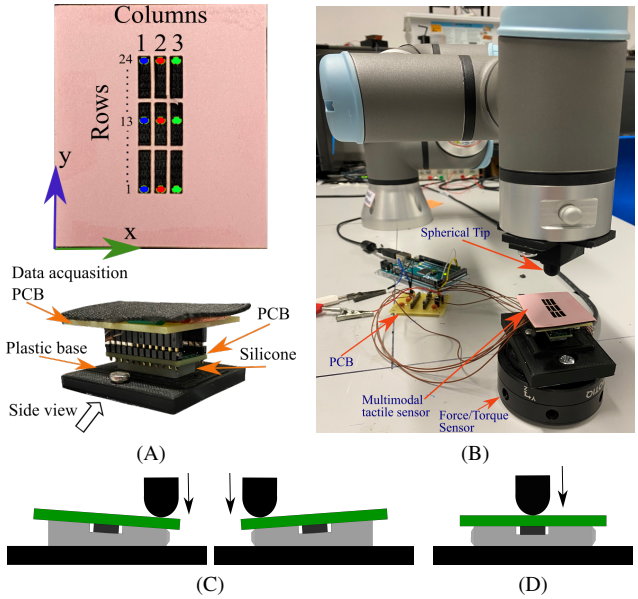

Fig. 3. Sensor and robot setup. (A) Multimodal tactile sensor covered with elastic fabric (bottom), and array of 3 columns and 24 rows for data collection (top). (B) Robotic setup used for tactile data collection. (C) The robot taps on the tactile sensor along 24 contact positions on each column (side view). (D) Data collection on top of the sensing element for sensitivity analysis (side view).

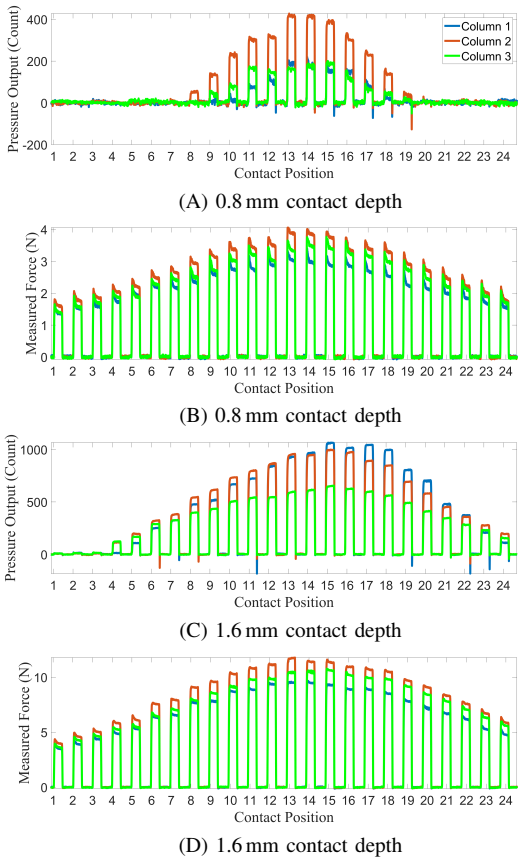

Fig. 4. Pressure data along the 24 rows of each column of the tactile sensor. (A) Mean pressure output for all contact points at 0.8 mm contact depth. (B) Mean measured force values for all contact points on z axis at 0.8 mm contact depth. (C) Mean pressure output for all contact points at 1.6 mm contact depth. (D) Mean measured force values for all contact points on z axis at 1.6 mm contact depth.

the chip is located on the PCB. The experimental setup in Figure 3B is used for the analysis of the sensor sensitivity, where pressure output from the tactile sensor and force measured with the FT-300 force/torque sensor are sampled at 30 Hz and 100 Hz, respectively, and sent to a workstation. In this experiments, the UR robot moves along the z axis to apply force on contact position 13 that corresponds to the position of the chip. The robot touches the sensor from contact depth 0.8 mm to 1.7 mm (the sensor output saturates) with 0.1 mm steps and 5 s contact duration at each step (Figure 3D). This process is repeated 30 times. After completing the data collection, the force/torque sensor data are down-sampled to match the number of samples from the tactile sensor.

The mean values of measured force and pressure output

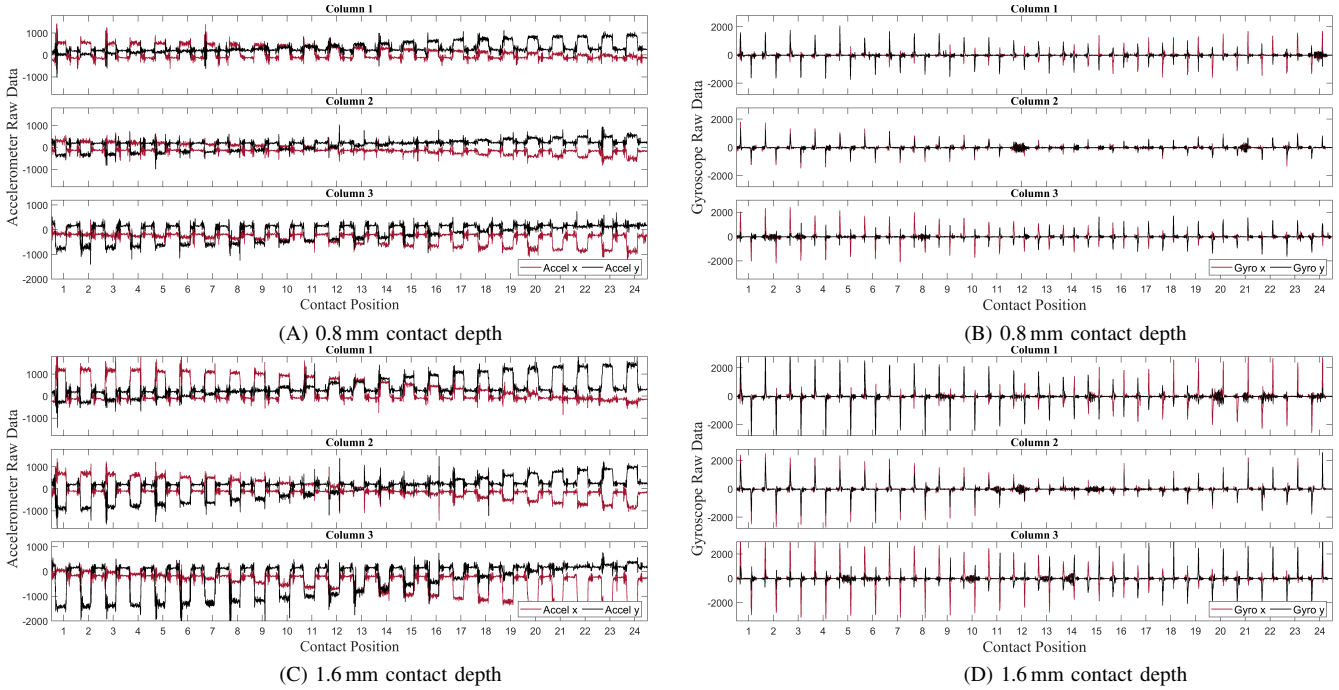

(A) 0.8 mm contact depth (B) 0.8 mm contact depth

(C) 1.6 mm contact depth (D) 1.6 mm contact depth

Fig. 5. Accelerometer and gyroscope signals on the x and y axes along the 24 rows of each column of the tactile sensor. (A)-(B) Mean accelerometer and gyroscope signals for all contact points in Columns 1, 2 and 3 on x and y axes at 0.8 mm contact depth. (C)-(D) Mean accelerometer and gyroscope signals for all contact points in Columns 1, 2 and 3 on x and y axes at 1.6 mm contact depth.

data are used for the sensitivity analysis of the tactile sensor. This data is shown in Figure 6A, which presents a quasi-linear increment of pressure output from 263 to 969 counts for force values from 3.53 N to 13 N. The change in measured force for contact depths ranging from 0.8 mm to 1.7 mm are shown in Figure 6B. The second order polynomial function from the measured force and pressure data from the highest sensitive position of the tactile sensor (contact position 13) is shown in Figure 6C. The polynomial function employed is as follows:

$$F(p) = 5.844e^{-6}.p^2 + 0.0041.p + 2.3304 \qquad (1)$$

where F is the estimated force and p is the pressure output from the sensor. The polynomial function exhibits $R^2 = 94\%$.

Finite Element Analysis (FEA) is used to compare the simulation results with the experimental data from the sensitive contact position of the sensor. In the simulation, force is applied on the center of the tactile sensor, which corresponds to contact position 13 of the real sensor. The tactile sensor model used in FEA analysis is shown in Figure 7, which represents the real sensor described in Section III-B. The FEA analysis shows the compression of the silicon material

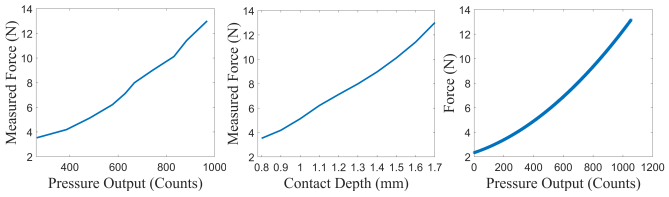

(A) (B) (C)

Fig. 6. Tactile sensor response to force applied at different contact depths. (A) Mean pressure output against measured force. (B) Contact depths against mean measured force. (C) Estimated force using a second order polynomial function.

under simulated forces. The nonlinear elastic response of the Ecoflex 00-30 material is described using a version of constitutive Yeoh model for compressible rubbers. The strain energy density function of this model is represented as follows:

$$W = \sum_{i=1}^{N} C_i(\overline{I}_1 - 3)^i + \sum_{k=1}^{N} D_i(J-1)^{2k} \qquad (2)$$

where $\overline{I}_1 = J^{-2/3}$, and C_i and D_i are material constants. Constant parameters for Ecoflex 00-30 used in the FEA analysis are $C_1 = 17$ kPa, $C_2 = -0.2$ kPa, $C_3 = 0.023$ kPa, $D_1 = 15$, $D_2 = 20$, and $D_3 = 10$, which are obtained under uniaxial compressible experiments in third order ($N = 3$) [38]. In simulation, force is applied on the top of the sensor, while compressing the sensor to contact depth of 1.7 mm, which corresponds to the maximum contact depth used in the sensory sensitive experiment. The contour plot of the von Mises stress and results of compressing the sensor at 0.85 mm, 1.3 mm and 1.7 mm are shown in Figures 7A and 7B, respectively. Sensor compression between 0.85 mm and 1.7 mm is used for force prediction and comparison with experimental results. Stress values from the centre of the sensor (red frame) are used to calculate the force values. The force applied on the sensor can be calculated using the von Mises stress as follows:

$$Stress = \frac{Force}{Area}. \qquad (3)$$

For example, if the sensor is compressed at 0.85 mm, the stress value of the centre of the sensor is 0.012 MPa and the surface area of the silicon covering the sensor is $11.5\,\text{mm} \times 24\,\text{mm} = 276\,\text{mm}^2$, then the predicted force is 3.31 N. Figure 7B shows the experimental (blue curve) and predicted force (red curve) values for different compression

values or contact depths applied on the tactile sensor. Experimental and predicted force at contact depth of 1.7 mm are 13 N and 14.6 N, respectively, whereas for the minimum contact depth of 0.8 mm, the experimental and predicted force values are 3.5 N and 3.3 N, respectively. For the contact depth of 1.3 mm, the value of 8 N is observed for both the experimental and predicted force.

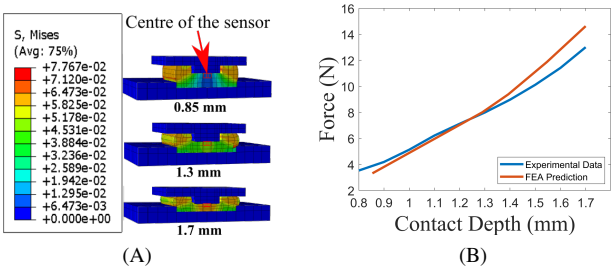

Fig. 7. FEA analysis of the tactile sensor. (A) Tactile sensor compressed at different contact depths. (B) Predicted force applied on the sensor for different contact depths.

IV. Experiments and Results

In this section, the capability of the multimodal tactile sensor for estimation of contact location and robot control are tested in offline and real-time modes.

A. Contact Location Estimation in Offline Mode

The capability of the multimodal tactile sensor to estimate where it is being touched is tested in offline mode using accelerometer and gyroscope data. This type of data, together with different computational methods and robot platforms, has shown to be accurate for detection of contact location [35], [39]. For this experiment, data is collected from an array of 3 columns×24 rows based on a tapping exploratory procedure on the tactile sensor, with a range of contact depths from 0.2 mm to 1.6 mm and 0.2 mm steps as described in Section III-C. This process is systematically performed and repeated 5 times using the UR robot platform. The data collected from the 24 rows are segmented into 3 groups of 8 rows each to create the array of 3×3 contact regions or classes for recognition with the tactile sensor (a total of 9 contact regions) as shown in Figure 8A. The recognition of this array of contact regions with our tactile sensor is possible by the use of multimodal data together with computational methods. Each of the 9 contact regions is composed of 38 samples of x- and y signals from accelerometer and gyroscope, creating a data matrix of 4 signals×38 samples. The size of the dataset of each contact depth is augmented adding Gaussian noise (30 dB signal-to-noise ratio) from 5 to 105. Each contact region consists of 840 data matrices from one contact depth, and totally including data from 8 different contact depths, each contact region has 6720 data matrices.

This dataset is used as input data to the CNN model shown in Figure 8B, where the feature learning layer is composed of one convolutional layer with 3×3 filter size, a ReLU activation function and max-pooling. The output of this layer is connected to the classification layer, where the input data is flattened and sent of a fully connected layer with 320 neurons, followed by the softmax function with 9 output neurons that output the probability of being touched each of the 9 contact regions defined on the tactile sensor. The training and testing of the CNN model use 80% and 20% of samples from the dataset, respectively. This process is performed using data from each contact depth individually and also combining the data from all contact depths to analyse which case provides better recognition of contact regions. This recognition process is repeated 10 times to analyse the robustness of the data and recognition method. A k-fold cross validation (with k=5 folds) is also performed to analyse the robustness of the recognition process. The mean accuracy results in Table I, show that large contact depths provide strong acceleration and gyroscope signals, resulting in a higher accuracy for estimation of contact location on the sensor. Thus, small and larger contact depths of 0.2 mm and 1.6 mm achieved 84.7% and 98.9% mean accuracy for 10 times trial, and 86.9% and 99.4% mean accuracy for k-fold cross validation method, respectively. For the case when all contact depths were used with the CNN model, the recognition accuracy was affected by the low accuracy from small contact depths. Mean accuracy and standard deviation obtained by k-fold cross validation method are slightly higher than the mean accuracy and standard deviation of 10 times trial. However, the mean accuracy from the 10 trials of training and testing performed for all cases was 93.1%, while the mean accuracy from k-fold cross validation for all cases was 89.7%. Figure 8C presents the confusion matrix which shows that the recognition errors mainly occurred at the middle contact regions of the multimodal tactile sensor.

B. Contact Location Estimation in Real-time

The multimodal tactile sensor is also validated in real-time mode with experiments for estimation of the contact location and robot control. For the recognition of contact location, data is systematically collected from the 9 contact regions using the UR robot platform. The contact depth for this process is set to 1.2 mm which provided a reliable recognition accuracy in the offline experiment. The robot is programmed using MoveIt motion planning libraries to perform a tapping exploratory procedure on each contact region of the sensor with a duration of 3s per tap to collect accelerometer and gyroscope signals (Figure 9A). This data is prepared into 4×38 matrices, as described in Section IV-A, to be used as input to the CNN model for recognition of contact location in real-time. The data collected from the sensor is sent to a workstation using ROS and processed by the CNN model developed in MATLAB.

TABLE I
Classification Accuracy for Each Contact Depth and Combination of All Contact Depths Using a CNN.

Contact Depth	10 times trial		5-fold cross validation	
	Mean Accuracy	Standard Deviation	Mean Accuracy	Standard Deviation
0.2 mm	84.7%	0.8%	86.9%	4.08%
0.4 mm	84.7%	1%	90.6%	4.04%
0.6 mm	89.5%	1.08%	95.4%	3.19%
0.8 mm	94.2%	1.07%	96.8%	2.22%
1.0 mm	95.9%	1.64%	97.9%	2.3%
1.2 mm	97.7%	0.55%	98.4%	0.68%
1.4 mm	97.7%	0.69%	98.8%	1.11%
1.6 mm	98.9%	0.42%	99.4%	0.89%
All cases	93.1%	0.86%	89.6%	6.16%

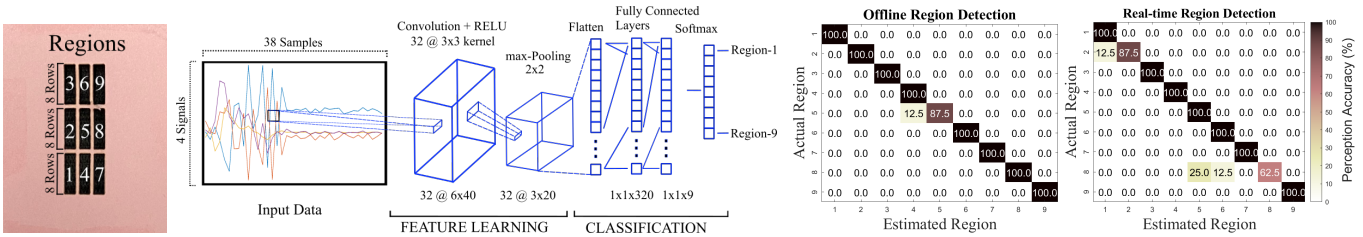

(A) Sensor regions (B) Structure of CNN (C) All cases combined (D) Real Time

Fig. 8. (A) A paper showing the contact areas corresponding to the size of the silicon is placed on the elastic fabric. (B) CNN model is composed of one convolutional and max-pooling layer, followed by flatten, two fully connected layers and softmax layer. Input data is created from accelerometer and gyroscope signals on x and y axis. The CNN estimates the area of the applied contact. (C) Confusion matrix showing the accuracy of contact location estimation for all cases and (D) real-time experiment at 1.2 mm contact depth.

The recognition process achieved accuracy of 93% and the recognition accuracy of each contact region is shown in the confusion matrix in Figure 8D.

The capability of the tactile sensor for robot control is also evaluated in real-time. In this experiment, the UR robot arm is controlled to move to a specific position on a grid according to the contact region of the tactile sensor touched by the user (Figure 9B). For this process, the CNN model trained with the data from all contact depths is used to recognise which contact region has been touched. The user touched each of the 9 contact regions on the tactile sensor using a mini screwdriver tool. Accelerometer and gyroscope data are collected when the pressure output of the sensor resulting of the applied contact exceeds a predefined threshold. This data is grouped into a 4×38 matrix as explained in Section IV-A. Once the data is collected, it is sent to MATLAB via ROS to be processed by the CNN model. The region recognised by the CNN is mapped to a predefined robot position on a grid displayed in a screen. The steps of this experiment is as follows: 1) the robot is set to home position and waits in its current position until a contact is detected on the multimodal tactile sensor, 2) when the user touches the sensor, the trained CNN model processes the sensor data to recognise the contact region being touched, and 3) this output is used to move the robot to the corresponding position. For instance, if a contact on the first sensor region is detected, the UR robot is controlled to move from the current home position to position 1 on a grid displayed in a screen (Figure 9B). This experiment was completed successfully, demonstrating that the multimodal tactile sensor can detect where it has been touched and use this information for robot control.

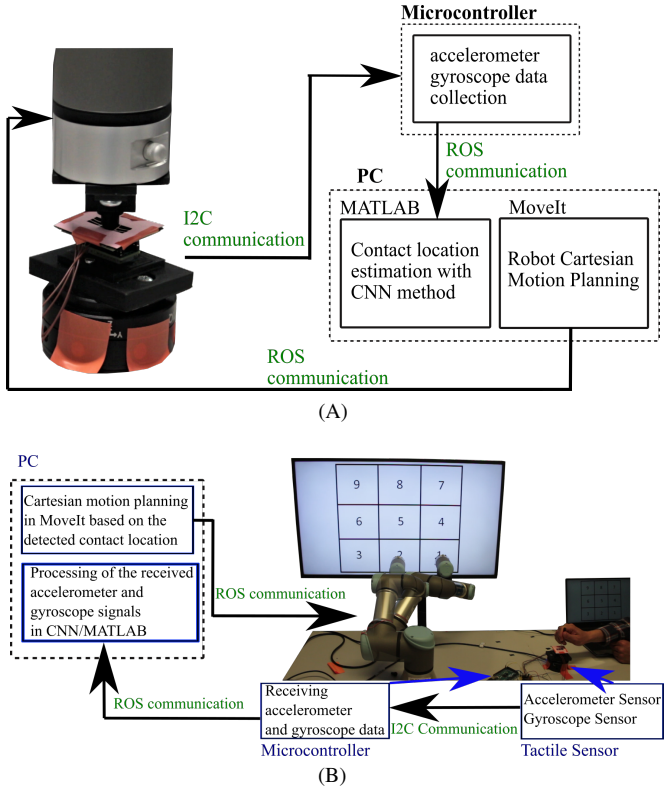

Fig. 9. (A) Contact location estimation in real-time. (B) Robot position control based on the perception of contact location on the tactile sensor.

V. Discussion

A low-cost multimodal tactile sensor capable of providing accelerometer, gyroscope and pressure data has been presented in this paper. Multimodal data are obtained using only one sensing element (ICM-20789 chip) for fabrication of the tactile sensor. To our knowledge, this is the first work using this chip for the development of a tactile sensor which contrast to previous works commonly used MPL115A2, BMP280 chips. The sensor was covered with a soft rectangular case after systematically investigating, testing and validating different design approaches to ensure accurate sensor response. In the first design approach, the chip was cast in liquid rubber Vytaflex 20 [20] to form a stiff contact surface. The chip and rubber were placed in a vacuum chamber to extract the air trapped in the chip through the ventilation orifice. Even though the tactile sensor provided stable gyroscope and accelerometer data, strong drift and saturation on pressure data were observed, making the sensor unstable and unreliable for touch sensing. In the second design approach, the lid of the chip was removed to enlarge the ventilation orifice from 0.3 mm to 1.0 mm to fix the signal drift and saturation issues following the process in [23]. The lid was placed back, glued it and cast in rubber. This approach did not show improvement in the signal drift and saturation. In the third design approach, the chip was covered with an empty rectangular case made of Vytaflex 30 [33]. The case was formed pouring rubber material in a plastic mould, curing the rubber at room temperature, and gluing it on the PCB to cover the chip. This approach provided a stable sensor signal, fixing the issues of signal drift and saturation. However, the

sensor did not show a sensitive response in accelerometer and gyroscope data when force was applied on the rectangular rubber case. Therefore, a fourth design approach was implemented using Ecoflex 00-30 rubber to cover the PCB and chip. This approach fixed the signal drift and saturation issues, and showed a clear change in accelerometer and gyroscope signals increasing the sensing area of the chip and improving the spatial impulse response and sensitivity of the sensor. This systematic analysis performed in this study offers the most suitable design approach for the development of multimodal tactile sensors using the ICM-20789 sensing element. The experiments showed that the sandwich design provided higher spatial impulse response compared to the barometric based tactile sensors [20], [21], [22], [23], [25]. The use of one chip in the soft bendable structure reduces the design and data acquisition complexity reading data simultaneously from IMU and barometric sensors compared to the works [25], [26] rely on mechanical components such as springs for bending, and multiple separate sensing elements to read multimodal data.

The sensitivity analysis showed that the centre of the tactile sensor provides the highest sensitivity (force between 3.53 N and 13 N). This suggests that this tactile sensor might not respond to contact force smaller than 3.53 N. However, this contact detection threshold can be improved designing the soft rectangular case of the sensor with different thickness, size and rubber. Force values were calculated using the stress results from the center of the sensor in the FEA under the different contacts depths. Calculated force values from FEA and force values obtained from the Equation 1 showed similar behaviour for small contact depths (0.8 mm to 1.3 mm), and a slight difference for larger contact depths (1.4 mm to 1.7 mm).

The tactile sensor data were segmented into 9 regions or classes and used with CNN methods for recognition of contact location in offline mode. The training and testing processes showed that accelerometer and gyroscope data allowed the CNN to achieve the highest recognition accuracy. The use of pressure data did not show an improvement in the recognition process, which relates to similarities in pressure data along the sensor. The training results showed that the recognition accuracy improved for large contact depths (98.9% and 99.4% at 1.6 mm depth for 10 times trial and cross validation respectively), which is related to larger changes in accelerometer and gyroscope data. Contact location recognition in real-time was performed using a robot arm and the CNN trained with data from 1.2 mm contact depth, which achieved one of the high accuracies in the offline analysis. The recognition accuracy in real-time for all 9 regions was 93% and the accuracy for each individual region is shown in the confusion matrix in Figure 8D. The recognition errors mainly occurred at contact locations close to the transition between regions, given that data overlapped from two consecutive regions.

Our multimodal sensor is capable of providing tactile data from a large surface using one chip or sensing element. We have shown in [40] that the tactile sensor can be used to cover larger areas with a robotic finger forming a multimodal sensing area of 65 mm x 34.5 mm. The multiple data available in these tactile sensors placed in the robotic finger have been used for grasping objects and handover applications in [41]. Our approach reduces the design and data collection complexity and cost compared to sensing devices composed of separate sensing elements used to cover large areas of robots. Moreover, the use of this multimodal tactile sensor together with machine learning allows the rearranging of the sensor data layout to estimate a different number of contact locations (e.g., 2x2, 3x3) compared to methods that require fixed arrays of sensing elements [42], [43]. We have used accelerometer and gyroscope signals with CNN models for detection of contact location motivated by previous works on contact estimation [35], [39]. In the current sensor configuration, only one contact location can be detected at a time. Contact detection and the estimation of the contact location using multimodal data have been validated controlling the position of the UR robot arm. This application is useful for other applications such as teleoperation [44]. Other applications that we plan to explore for the future work are the recognition of textures, materials and objects, as well as covering larger surfaces including robotic limbs and torso.

Overall, this paper has presented a novel tactile sensor composed of a new sensing element, a systematic analysis of sensor design based on a sandwich structure approach and multimodal data processing using machine learning for contact detection and location estimation for robot control in real-time.

VI. Conclusions

In this paper, we presented a low-cost multimodal tactile sensor capable of providing pressure, accelerometer and gyroscope data for robotic sensing, exploration, perception and control. The sensor was built using a single sensing element and soft rubber material. The spatial impulse response, sensitivity and mechanical response of the sensor were analysed systematically using a robot platform and Finite Element Analysis. The tactile sensor was validated with experiments in offline and real-time modes for detection of contact, recognition of contact location and robot control using a Convolutional Neural Network. The sensor demonstrated to be capable of recognising contact location accurately for control of a robot arm. Overall, this work offers an alternative and low-cost approach for multimodal tactile sensing suitable for applications in robot exploration, control and interaction.

References

[1] F. Flacco, T. Kröger, A. De Luca, and O. Khatib, "A depth space approach to human-robot collision avoidance," in *2012 IEEE international conference on robotics and automation*. IEEE, 2012, pp. 338–345.

[2] J. Male and U. Martinez-Hernandez, "Collaborative architecture for human-robot assembly tasks using multimodal sensors," in *2021 20th International Conference on Advanced Robotics (ICAR)*. IEEE, 2021, pp. 1024–1029.

[3] A. Yamaguchi and C. G. Atkeson, "Combining finger vision and optical tactile sensing: Reducing and handling errors while cutting vegetables," in *2016 IEEE-RAS 16th International Conference on Humanoid Robots (Humanoids)*. IEEE, 2016, pp. 1045–1051.

[4] M. Fritzsche, N. Elkmann, and E. Schulenburg, "Tactile sensing: A key technology for safe physical human robot interaction," in *Proceedings of the 6th International Conference on Human-robot Interaction*, 2011, pp. 139–140.

[5] G. A. Al, P. Estrela, and U. Martinez-Hernandez, "Towards an intuitive human-robot interaction based on hand gesture recognition and proximity sensors," in *2020 IEEE International Conference on Multisensor Fusion and Integration for Intelligent Systems (MFI)*. IEEE, 2020, pp. 330–335.

[6] R. S. Dahiya, P. Mittendorfer, M. Valle, G. Cheng, and V. J. Lumelsky, "Directions toward effective utilization of tactile skin: A review," *IEEE Sensors Journal*, vol. 13, no. 11, pp. 4121–4138, 2013.

[7] Z. Kappassov, J.-A. Corrales, and V. Perdereau, "Tactile sensing in dexterous robot hands," *Robotics and Autonomous Systems*, vol. 74, pp. 195–220, 2015.

[8] R. S. Dahiya, G. Metta, M. Valle, and G. Sandini, "Tactile sensing—from humans to humanoids," *IEEE transactions on robotics*, vol. 26, no. 1, pp. 1–20, 2009.

[9] A. Schmitz, P. Maiolino, M. Maggiali, L. Natale, G. Cannata, and G. Metta, "Methods and technologies for the implementation of large-scale robot tactile sensors," *IEEE Transactions on Robotics*, vol. 27, no. 3, pp. 389–400, 2011.

[10] J. M. Romano, K. Hsiao, G. Niemeyer, S. Chitta, and K. J. Kuchenbecker, "Human-inspired robotic grasp control with tactile sensing," *IEEE Transactions on Robotics*, vol. 27, no. 6, pp. 1067–1079, 2011.

[11] A. Rana, J.-P. Roberge, and V. Duchaine, "An improved soft dielectric for a highly sensitive capacitive tactile sensor," *Ieee sensors journal*, vol. 16, no. 22, pp. 7853–7863, 2016.

[12] C. Chi, X. Sun, N. Xue, T. Li, and C. Liu, "Recent progress in technologies for tactile sensors," *Sensors*, vol. 18, no. 4, p. 948, 2018.

[13] A. Drimus, G. Kootstra, A. Bilberg, and D. Kragic, "Design of a flexible tactile sensor for classification of rigid and deformable objects," *Robotics and Autonomous Systems*, vol. 62, no. 1, pp. 3–15, 2014.

[14] D. Goger, N. Gorges, and H. Worn, "Tactile sensing for an anthropomorphic robotic hand: Hardware and signal processing," in *2009 IEEE International Conference on Robotics and Automation*. IEEE, 2009, pp. 895–901.

[15] S. Pohtongkam and J. Srinonchat, "Tactile object recognition for humanoid robots using new designed piezoresistive tactile sensor and dcnn," *Sensors*, vol. 21, no. 18, p. 6024, 2021.

[16] P. Kampmann and F. Kirchner, "Integration of fiber-optic sensor arrays into a multi-modal tactile sensor processing system for robotic end-effectors," *Sensors*, vol. 14, no. 4, pp. 6854–6876, 2014.

[17] B. Ward-Cherrier, N. Pestell, L. Cramphorn, B. Winstone, M. E. Giannaccini, J. Rossiter, and N. F. Lepora, "The tactip family: Soft optical tactile sensors with 3d-printed biomimetic morphologies," *Soft robotics*, vol. 5, no. 2, pp. 216–227, 2018.

[18] C. Ledermann, S. Wirges, D. Oertel, M. Mende, and H. Woern, "Tactile sensor on a magnetic basis using novel 3d hall sensor-first prototypes and results," in *2013 IEEE 17th International Conference on Intelligent Engineering Systems (INES)*. IEEE, 2013, pp. 55–60.

[19] G. d. Boer, N. Raske, H. Wang, J. Kow, A. Alazmani, M. Ghajari, P. Culmer, and R. Hewson, "Design optimisation of a magnetic field based soft tactile sensor," *Sensors*, vol. 17, no. 11, p. 2539, 2017.

[20] Y. Tenzer, L. P. Jentoft, and R. D. Howe, "The feel of mems barometers: Inexpensive and easily customized tactile array sensors," *IEEE Robotics & Automation Magazine*, vol. 21, no. 3, pp. 89–95, 2014.

[21] M. Y. Chuah and S. Kim, "Enabling force sensing during ground locomotion: A bio-inspired, multi-axis, composite force sensor using discrete pressure mapping," *IEEE Sensors Journal*, vol. 14, no. 5, pp. 1693–1703, 2014.

[22] F. Ruppert and A. Badri-Spröwitz, "Foottile: a rugged foot sensor for force and center of pressure sensing in soft terrain," in *2020 IEEE International Conference on Robotics and Automation (ICRA)*. IEEE, 2020, pp. 4810–4816.

[23] R. Koiva, T. Schwank, G. Walck, M. Meier, R. Haschke, and H. Ritter, "Barometer-based tactile skin for anthropomorphic robot hand," 2020.

[24] N. Wettels, J. A. Fishel, and G. E. Loeb, "Multimodal tactile sensor," in *The Human Hand as an Inspiration for Robot Hand Development*. Springer, 2014, pp. 405–429.

[25] T. E. A. De Oliveira, A.-M. Cretu, and E. M. Petriu, "Multimodal bio-inspired tactile sensing module," *IEEE Sensors Journal*, vol. 17, no. 11, pp. 3231–3243, 2017.

[26] S. Ottenhaus, P. Weiner, L. Kaul, A. Tulbure, and T. Asfour, "Exploration and reconstruction of unknown objects using a novel normal and contact sensor," in *2018 IEEE/RSJ International Conference on Intelligent Robots and Systems (IROS)*. IEEE, 2018, pp. 1614–1620.

[27] P. Mittendorfer and G. Cheng, "Humanoid multimodal tactile-sensing modules," *IEEE Transactions on robotics*, vol. 27, no. 3, pp. 401–410, 2011.

[28] D. S. Chathuranga, Z. Wang, A. Mitani, S. Hirai *et al.*, "A biomimetic soft fingertip applicable to haptic feedback systems for texture identification," in *2013 IEEE International Symposium on Haptic Audio Visual Environments and Games (HAVE)*. IEEE, 2013, pp. 29–33.

[29] K. Aquilina, D. A. Barton, and N. F. Lepora, "Principal components of touch," in *2018 IEEE International Conference on Robotics and Automation (ICRA)*. IEEE, 2018, pp. 4071–4078.

[30] J. Lin, R. Calandra, and S. Levine, "Learning to identify object instances by touch: Tactile recognition via multimodal matching," in *2019 International Conference on Robotics and Automation (ICRA)*. IEEE, 2019, pp. 3644–3650.

[31] A. Albini, S. Denei, and G. Cannata, "Human hand recognition from robotic skin measurements in human-robot physical interactions," in *2017 IEEE/RSJ International Conference on Intelligent Robots and Systems (IROS)*. IEEE, 2017, pp. 4348–4353.

[32] U. Martinez-Hernandez, A. Damianou, D. Camilleri, L. W. Boorman, N. Lawrence, and T. J. Prescott, "An integrated probabilistic framework for robot perception, learning and memory," in *2016 IEEE International Conference on Robotics and Biomimetics (ROBIO)*. IEEE, 2016, pp. 1796–1801.

[33] G. A. Al and U. Martinez-Hernandez, "A low-cost compact soft tactile sensor with a multimodal chip," in *International Conference on Advanced Robotics, 2021*, 2021.

[34] S. Luo, W. Mou, K. Althoefer, and H. Liu, "Novel tactile-sift descriptor for object shape recognition," *IEEE Sensors Journal*, vol. 15, no. 9, pp. 5001–5009, 2015.

[35] Y. Iwamoto, R. Meattini, D. Chiaravalli, G. Palli, K. Shibuya, and C. Melchiorri, "A low cost tactile sensor for large surfaces based on deformable skin with embedded imu," in *2020 IEEE Conference on Industrial Cyberphysical Systems (ICPS)*, vol. 1. IEEE, 2020, pp. 501–506.

[36] J. M. Gandarias, A. J. Garcia-Cerezo, and J. M. Gomez-de Gabriel, "Cnn-based methods for object recognition with high-resolution tactile sensors," *IEEE Sensors Journal*, vol. 19, no. 16, pp. 6872–6882, 2019.

[37] M. Alameh, Y. Abbass, A. Ibrahim, and M. Valle, "Smart tactile sensing systems based on embedded cnn implementations," *Micromachines*, vol. 11, no. 1, p. 103, 2020.

[38] D. Steck, J. Qu, S. B. Kordmahale, D. Tscharnuter, A. Muliana, and J. Kameoka, "Mechanical responses of ecoflex silicone rubber: Compressible and incompressible behaviors," *Journal of Applied Polymer Science*, vol. 136, no. 5, p. 47025, 2019.

[39] K.-W. Lee, S.-C. Kim, and S.-C. Lim, "Deeptouch: Enabling touch interaction in underwater environments by learning touch-induced inertial motions," *IEEE Sensors Journal*, vol. 22, no. 9, pp. 8924–8932, 2022.

[40] G. A. Al and U. Martinez-Hernandez, "A single-chip multimodal tactile sensor for a robotic gripper," in *International Conference on Advanced Robotics*, 2021.

[41] J. Male, G. A. Al, A. Shabani, and U. Martinez-Hernandez, "Multimodal sensor-based human-robot collaboration in assembly tasks." IEEE, 2022 (In press).

[42] A. Cirillo, F. Ficuciello, C. Natale, S. Pirozzi, and L. Villani, "A conformable force/tactile skin for physical human–robot interaction," *IEEE Robotics and Automation Letters*, vol. 1, no. 1, pp. 41–48, 2015.

[43] G. Pang, J. Deng, F. Wang, J. Zhang, Z. Pang, and G. Yang, "Development of flexible robot skin for safe and natural human–robot collaboration," *Micromachines*, vol. 9, no. 11, p. 576, 2018.

[44] Y. Yan, Z. Hu, Z. Yang, W. Yuan, C. Song, J. Pan, and Y. Shen, "Soft magnetic skin for super-resolution tactile sensing with force self-decoupling," *Science Robotics*, vol. 6, no. 51, p. eabc8801, 2021.

Gorkem Anil Al received his MSc degree in Robotics from the University of Bristol, and Bristol Robotics Lab, UK, in 2017. He is currently a PhD student in the Department of Electronic and Electrical Engineering, and the Centre for Autonomous Robotics (CENTAUR), the University of Bath, UK. His research interests include haptic technologies, robot sensing and perception, machine learning and human-robot interaction.

Uriel Martinez-Hernandez received the PhD degree from the Department of Automatic Control and Systems Engineering, University of Sheffield, Sheffield, UK, in 2015. He is currently a Lecturer (Assistant Professor) in Robotics and Autonomous Systems at the Centre for Autonomous Robotics (CENTAUR), University of Bath, UK. His research interests include active perception with touch and vision, machine learning for autonomous robots, human-robot interaction and wearable assistive robotics.